

Linear-Cost Vecchia Approximation of Multivariate Normal Probabilities

Jian Cao*

Matthias Katzfuss[†]

Abstract

Multivariate normal (MVN) probabilities arise in myriad applications, but they are analytically intractable and need to be evaluated via Monte-Carlo-based numerical integration. For the state-of-the-art minimax exponential tilting (MET) method, we show that the complexity of each of its components can be greatly reduced through an integrand parameterization that utilizes the sparse inverse Cholesky factor produced by the Vecchia approximation, whose approximation error is often negligible relative to the Monte-Carlo error. Based on this idea, we derive algorithms that can estimate MVN probabilities and sample from truncated MVN distributions in linear time (and that are easily parallelizable) at the same convergence or acceptance rate as MET, whose complexity is cubic in the dimension of the MVN probability. We showcase the advantages of our methods relative to existing approaches using several simulated examples. We also analyze a groundwater-contamination dataset with over twenty thousand censored measurements to demonstrate the scalability of our method for partially censored Gaussian-process models.

Keywords: censored Gaussian process; integration variable reordering; minimax exponential tilting; truncated multivariate normal; sparse inverse Cholesky approximation

1 Introduction

Multivariate normal (MVN) probabilities, which are integrals over MVN densities, must be evaluated in a variety of settings, most notably those involving Gaussian processes (GPs), including GP regression with inequality constraints (Da Veiga and Marrel, 2012), joint threshold-exceedance probabilities for GPs (Bolin and Lindgren, 2015), probit GP models for binary responses (Durrante, 2019), skew-normal models (Zhang and El-Shaarawi, 2010), and censored scale-mixtures of normals for modeling tail dependence (Huser et al., 2017). However, MVN probabilities are analytically intractable, and direct application of numerical integration rules often leads to highly inaccurate estimates (Genz, 1992).

Current computational approaches for MVN probabilities are mostly based on the separation of variable (SOV) method (Genz, 1992). SOV applies a series of transformations such that the MVN probability can be written as an expectation of quantities with low variance, allowing an

*Department of Mathematics, University of Houston. jcao21@uh.edu

[†]Department of Statistics, University of Wisconsin–Madison. katzfuss@gmail.com

approximation of the expectation as the average of Monte Carlo samples. SOV consists of two stages: in the pre-processing stage, the Cholesky factor of the $n \times n$ MVN covariance matrix is computed in $\mathcal{O}(n^3)$ time; in the MC sampling stage, N samples are drawn, each in $\mathcal{O}(n^2)$ time. The resulting SOV time complexity is $\mathcal{O}(n^3 + Nn^2)$. To improve upon the original SOV method, Genz and Bretz (2009) introduced a univariate variable reordering technique used in the pre-processing stage that produces the Cholesky factor and further reduces the MC variance. Based on the series of integrand transformation used in the SOV method, Botev (2017) used importance sampling with minimax exponentially tilted (MET) normal proposal densities during the MC sampling stage to reduce variance. This results in substantially higher accuracy for tail MVN probabilities than Genz and Bretz (2009), but it requires iterative optimization of the proposal density in the pre-processing stage at a per-iteration complexity of $\mathcal{O}(n^3)$; in practice, this optimization is often more expensive than the MC sampling. Sampling from truncated MVN (TMVN) distributions is closely connected to approximating MVN probabilities (Botev, 2017). Specifically, the integrand in MET (or SOV) can be decomposed into two parts that can be viewed as a proposal density and a density ratio, which can be used for importance sampling from TMVN distributions at the same cost as estimating the corresponding MVN probability. MET is currently the state-of-the-art in terms of achieving the highest accuracy for estimating MVN probabilities and the highest acceptance rate for sampling TMVN distributions.

For evaluating high-dimensional MVN probabilities with spatial covariance matrices, Genton et al. (2018) and Cao et al. (2021) used hierarchical-matrix approximations to reduce the complexity of pre-processing and MC sampling for SOV by a factor of $n^{1/2}$. Other recent approaches for spatial MVN probabilities have used versions of the Vecchia approximation (Vecchia, 1988), which decomposes a multivariate density into a product of univariate conditional densities with small conditioning sets. Saha et al. (2022) applied a Vecchia-type approximation to reduce the complexity of computing the Cholesky factor in the preprocessing stage, but its per-sample complexity remains as $\mathcal{O}(n^2)$. Nascimento and Shaby (2022) decomposed the n -dimensional MVN probability into a product of lower-dimensional MVN probability ratios through assuming conditional independence in the MVN cumulative distribution function (CDF); while this is based on a similar principle as the Vecchia approximation, it appears that the screening effect (Stein, 2011) is weaker for MVN CDFs than for densities, resulting in substantially increased approximation error for CDF approximations.

Our proposed methods are also based on the Vecchia approximation, which makes a sparse-directed-acyclic-graph assumption. A Vecchia approximation of a MVN distribution results in a valid MVN distribution that has a covariance matrix with a sparse inverse Cholesky factor (Datta et al., 2016; Katzfuss and Guinness, 2021). Vecchia approximations can provide asymptotically exact inference in near-linear time for GPs with Matérn-type kernels up to boundary effects (Schäfer et al., 2021). Numerically, Vecchia approximations have been shown to be highly accurate even with small conditioning-set sizes in many settings, including spatial statistics and high-dimensional and multi-output GPs (e.g., Cao et al., 2022b, 2023; Datta et al., 2016; Jimenez and Katzfuss, 2023; Kang and Katzfuss, 2023; Katzfuss and Guinness, 2021; Katzfuss et al., 2020, 2022; Schäfer et al., 2021; Stein et al., 2004). Vecchia approximations can be applied to any covariance matrix, and we expect them to be most accurate if the covariance can be viewed as a stationary kernel defined over some (potentially unknown) input space (Kang and Katzfuss, 2023).

We propose scalable evaluation of MVN probabilities and sampling from TMVN distributions in linear time by applying suitable Vecchia approximations to the MET approach. We show that

the dominant computations for MET and SOV are equivalent to calculating the conditional means and variances of the integration variables. We reduce the conditioning sets in these calculations via the Vecchia approximation. We take full advantage of Vecchia’s sparse inverse Cholesky factor when computing the transformed MET integrand as well as its gradient and Hessian, which allows us to optimize the MET proposal density and sample from TMVN distributions in linear time. We demonstrate numerically that the Vecchia approximation error can be negligible relative to the Monte-Carlo error, despite the $\mathcal{O}(n^2)$ complexity reduction of our method relative to MET. In addition, both the pre-processing and sampling stages of our method are parallelizable. We show that our proposed method facilitates model estimation and posterior inference for partially censored MVN models that offer substantial information gain over existing approaches, particularly in spatial and environmental applications involving censored responses.

The remainder of this document is organized as follows. In Section 2, we provide a review of the SOV and MET methods in a unified framework to set up the mathematical notation for our proposed method. In Section 3, we introduce our transformations of the SOV and the MET integrands to achieve linear complexity for MC sampling. In Section 4, we derive the gradient and Hessian of our transformed MET integrand and show that solving for the proposal density used in MET can be achieved in $\mathcal{O}(n)$ time. In Section 5, we use the Vecchia approximation to reduce the complexity of the univariate variable reordering (Genz and Bretz, 2009) from $\mathcal{O}(n^3)$ to $\mathcal{O}(n^2)$, and we propose an additional $\mathcal{O}(n)$ reordering variant. Section 6 provides numerical comparisons to existing methods for variable reordering, estimating MVN probabilities, and sampling TMVN distributions. Section 7 shows the effectiveness of our proposed method for the estimation and inference for partially censored MVN models with simulated and real datasets. Section 8 concludes. All proofs can be found in Appendix A. An R implementation of our methods for variable reordering, computing MVN probabilities, and sampling TMVN distributions, along with code to reproduce our results, can be found at https://github.com/JCatwood/TMVN_Vecchia.

2 SOV and MET from an Importance Sampling Perspective

The MVN probability in an n -dimensional hyperrectangle has the general expression of:

$$\begin{aligned} \Phi_n(\mathbf{a}, \mathbf{b}; \boldsymbol{\mu}, \boldsymbol{\Sigma}) &= \int_{\mathbf{a}}^{\mathbf{b}} \phi_n(\mathbf{x}; \boldsymbol{\mu}, \boldsymbol{\Sigma}) d\mathbf{x} \\ &= \int_{\mathbf{a}}^{\mathbf{b}} \frac{1}{(2\pi)^{n/2} |\boldsymbol{\Sigma}|^{1/2}} \exp\left(-\frac{1}{2}(\mathbf{x} - \boldsymbol{\mu})^\top \boldsymbol{\Sigma}^{-1}(\mathbf{x} - \boldsymbol{\mu})\right) d\mathbf{x}, \end{aligned} \quad (1)$$

where $\boldsymbol{\mu}$ and $\boldsymbol{\Sigma}$ are the mean and the covariance matrix of the MVN distribution, respectively; \mathbf{a} and \mathbf{b} are lower and upper integration limits defining the hyperrectangle; and $\phi_n(\cdot)$ is the MVN density function. MVN probabilities defined over a region bounded by hyperplanes can be transformed into (1) through linear transformation. Without loss of generality, $\boldsymbol{\mu}$ is assumed zero and omitted throughout this paper, as $\Phi_n(\mathbf{a}, \mathbf{b}; \boldsymbol{\mu}, \boldsymbol{\Sigma}) = \Phi_n(\mathbf{a} - \boldsymbol{\mu}, \mathbf{b} - \boldsymbol{\mu}; \mathbf{0}, \boldsymbol{\Sigma})$. In many applications, including spatial statistics and Gaussian processes, $\boldsymbol{\Sigma}$ is a kernel matrix whose (i, j) th entry $\Sigma_{i,j} = \mathcal{K}(\mathbf{s}_i, \mathbf{s}_j)$ is obtained by evaluating a covariance kernel \mathcal{K} at the pair of locations or inputs \mathbf{s}_i and \mathbf{s}_j corresponding to the i th and j th entry of \mathbf{x} .

Denoting the lower Cholesky factor of $\boldsymbol{\Sigma}$ by \mathbf{L} , such that $\boldsymbol{\Sigma} = \mathbf{L}\mathbf{L}^\top$, a series of integrand transformations that start with the integration variable transformation $\mathbf{x} = \mathbf{L}\mathbf{y}$ may offer a clear

overview of both SOV (Genz, 1992) and MET (Botev, 2017):

$$\begin{aligned}\Phi_n(\mathbf{a}, \mathbf{b}; \Sigma) &= \int_{\tilde{a}_1}^{\tilde{b}_1} \int_{\tilde{a}_2}^{\tilde{b}_2} \cdots \int_{\tilde{a}_n}^{\tilde{b}_n} \phi_n(\mathbf{y}; \mathbf{I}_n) d\mathbf{y} \\ &= \int_{\tilde{a}_1}^{\tilde{b}_1} \frac{\Phi(\tilde{b}_1) - \Phi(\tilde{a}_1)}{\Phi(\tilde{b}_1) - \Phi(\tilde{a}_1)} \phi(y_1) \cdots \int_{\tilde{a}_n}^{\tilde{b}_n} \frac{\Phi(\tilde{b}_n) - \Phi(\tilde{a}_n)}{\Phi(\tilde{b}_n) - \Phi(\tilde{a}_n)} \phi(y_n) d\mathbf{y},\end{aligned}\quad (2)$$

$$\begin{aligned}&= \int_{\tilde{a}_1}^{\tilde{b}_1} \frac{\Phi(\tilde{b}_1 - \gamma_1) - \Phi(\tilde{a}_1 - \gamma_1)}{\Phi(\tilde{b}_1 - \gamma_1) - \Phi(\tilde{a}_1 - \gamma_1)} \frac{\phi(y_1)}{\phi(y_1 - \gamma_1)} \phi(y_1 - \gamma_1) \cdots \\ &\quad \int_{\tilde{a}_n}^{\tilde{b}_n} \frac{\Phi(\tilde{b}_n - \gamma_n) - \Phi(\tilde{a}_n - \gamma_n)}{\Phi(\tilde{b}_n - \gamma_n) - \Phi(\tilde{a}_n - \gamma_n)} \frac{\phi(y_n)}{\phi(y_n - \gamma_n)} \phi(y_n - \gamma_n) d\mathbf{y},\end{aligned}\quad (3)$$

$$= E_{q(\mathbf{y}; \boldsymbol{\gamma})}[h(\mathbf{y}; \boldsymbol{\gamma})],$$

$$\text{with } \tilde{a}_i = \frac{a_i - \sum_{j=1}^{i-1} L_{ij} y_j}{L_{ii}}, \quad \tilde{b}_i = \frac{b_i - \sum_{j=1}^{i-1} L_{ij} y_j}{L_{ii}},$$

where $\boldsymbol{\gamma}$ are the parameters for the proposal density used in MET, and $\phi(\cdot)$ and $\Phi(\cdot)$ are the probability density function (PDF) and the cumulative probability function (CDF) of the univariate standard normal distribution, respectively. From the perspective of importance sampling, (2) and (3) correspond to the SOV and the MET methods, respectively. Specifically, MET samples \mathbf{y} from $q(\mathbf{y}; \boldsymbol{\gamma})$ and then approximates $E_{q(\mathbf{y}; \boldsymbol{\gamma})}[h(\mathbf{y}; \boldsymbol{\gamma})]$ by the sample average, where

$$q(\mathbf{y}; \boldsymbol{\gamma}) = \prod_i^n \frac{\mathbb{1}_{y_i \in (\tilde{a}_i, \tilde{b}_i)}}{\Phi(\tilde{b}_i - \gamma_i) - \Phi(\tilde{a}_i - \gamma_i)} \phi(y_i - \gamma_i),\quad (4)$$

$$h(\mathbf{y}; \boldsymbol{\gamma}) = \prod_i^n \left\{ \Phi(\tilde{b}_i - \gamma_i) - \Phi(\tilde{a}_i - \gamma_i) \right\} \frac{\phi(y_i)}{\phi(y_i - \gamma_i)} \mathbb{1}_{y_i \in (\tilde{a}_i, \tilde{b}_i)}.\quad (5)$$

Notice that $h(\mathbf{y}; \boldsymbol{\gamma})$ is actually the PDF ratio between $\phi_n(\mathbf{y}; \mathbf{I}_n)$ truncated in $\mathbf{a} \leq \mathbf{L}\mathbf{y} \leq \mathbf{b}$ and $q(\mathbf{y}; \boldsymbol{\gamma})$, up to a normalizing constant. Because sampling from $q(\mathbf{y}; \boldsymbol{\gamma})$ can be performed via sequential sampling from n univariate truncated normal distributions as implied by (4), we can sample from $\phi_n(\mathbf{y}; \mathbf{I}_n)$ truncated in $\mathbf{a} \leq \mathbf{L}\mathbf{y} \leq \mathbf{b}$ or equivalently, $\phi_n(\mathbf{x}; \Sigma)$ truncated in $[\mathbf{a}, \mathbf{b}]$, using importance sampling. SOV is a special case of MET when the exponential tilting parameters $\boldsymbol{\gamma} = \mathbf{0}$. Botev (2017) proposed to use

$$\hat{\boldsymbol{\gamma}} = \arg \min_{\boldsymbol{\gamma}} \max_{\mathbf{y}: \mathbf{a} \leq \mathbf{L}\mathbf{y} \leq \mathbf{b}} \log h(\mathbf{y}; \boldsymbol{\gamma}),\quad (6)$$

which minimizes the worst likelihood ratio if we are to draw samples from the TMVN distribution. Solving for $\hat{\boldsymbol{\gamma}}$ is discussed in Section 4.

3 Sampling at Linear Complexity

3.1 Conditional mean and variance under Vecchia

After the pre-processing stage, the dominating $\mathcal{O}(n^2)$ complexity in the MC sampling of both SOV and MET comes from the computation of \tilde{a}_i and \tilde{b}_i ; specifically, for each $i = 2, \dots, n$, one must compute $\sum_{j=1}^{i-1} L_{ij} y_j$, which can be shown to be equivalent to $E[x_i | \mathbf{x}_{1:i-1}]$:

PROPOSITION 1. Suppose $\mathbf{x} \sim \phi_n(\mathbf{x}; \Sigma)$, \mathbf{L} is the lower Cholesky factor of Σ , and $\mathbf{x} = \mathbf{L}\mathbf{y}$. Then

$$E[x_i | \mathbf{x}_{1:i-1}] = \sum_{j=1}^{i-1} L_{ij} y_j, \quad \text{Var}[x_i | \mathbf{x}_{1:i-1}] = L_{i,i}^2,$$

where we use the notation $\mathbf{x}_{i:j} = [x_i, x_{i+1}, \dots, x_j]^\top$.

Each conditional expectation and variance can be computed at sublinear complexity via the Vecchia approximation (Vecchia, 1988), which truncates the conditioning sets in the conditional densities to subsets of sizes no bigger than m :

$$f(\mathbf{x}) = f(x_1) \cdot f(x_2 | x_1) \cdots f(x_n | \mathbf{x}_{1:n-1}) \approx f(x_1) \cdot f(x_2 | x_{c(1)}) \cdots f(x_n | \mathbf{x}_{c(n)}),$$

where $f(\cdot)$ is a generic density and the conditioning set $c(i)$ is a subset of $\{1, \dots, i-1\}$ of size $\min(m, i-1)$. When f is the normal density, the Vecchia approximation amounts to

$$\phi_n(\mathbf{x}; \Sigma) \approx \phi(x_1; \eta_1, l_1^2) \cdot \phi(x_2; \eta_2, l_2^2) \cdots \phi(x_n; \eta_n, l_n^2),$$

where each $\eta_i = E[x_i | \mathbf{x}_{c(i)}]$ and $l_i^2 = \text{Var}[x_i | \mathbf{x}_{c(i)}]$ can be computed straightforwardly based on $\mathcal{O}(m^2)$ entries of Σ . Each conditioning set is typically chosen as the indices of the m nearest previously ordered neighbors. For covariances $\Sigma_{i,j} = \mathcal{K}(\mathbf{s}_i, \mathbf{s}_j)$ based on isotropic kernels, Euclidean distance between inputs \mathbf{s}_i and \mathbf{s}_j can be used to define nearest neighbors; for other covariance matrices, the correlation distance $(1 - |\rho_{ij}|)^{1/2}$ with $\rho_{ij} = \Sigma_{ij} / (\Sigma_{ii} \Sigma_{jj})^{1/2}$ implicitly selects neighbors in a suitable transformed input space (Kang and Katzfuss, 2023). The Vecchia approximation is based on the screening effect (Stein, 2002), which describes the phenomenon that the marginal information gain from far-away responses is often minimal after conditioning on nearby responses. Any Vecchia approximation of a MVN density results in a valid joint MVN density with the same mean but a (slightly) different covariance matrix that has a sparse inverse Cholesky factor. Specifically, Schäfer et al. (2021) showed that, for each $i = 1, \dots, n$, the nonzero entries in the i th column of the inverse Cholesky factor $\mathbf{V} = \mathbf{L}^{-\top}$ can be obtained as:

$$\mathbf{V}_{\bar{c}(i),i} = \mathbf{u}_i \mathbf{u}_{i,1}^{-1/2}, \quad \text{with } \mathbf{u}_i = (\Sigma_{\bar{c}(i),\bar{c}(i)})^{-1} \mathbf{e}_1,$$

where $\bar{c}(i) = [i, c(i)]^\top$ and \mathbf{e}_1 is a vector whose first entry is 1 and all other entries are zero. Hence, \mathbf{V} can be computed using $\mathcal{O}(nm^3)$ operations and its columns can be computed in parallel. Schäfer et al. (2021) also showed that the covariance matrix under the Vecchia approximation minimizes the KL divergence from the original MVN distribution subject to the implied sparsity constraint on the inverse Cholesky factor \mathbf{V} . Furthermore, Vecchia approximations can achieve ϵ -accurate approximations for Matérn-type kernels up to boundary effects using m that only grows polylogarithmically with n (Schäfer et al., 2021). Numerical evidence that a small $m \leq 50$ is typically sufficient for very large n is also abundant in the literature (see Section 1 for references). Therefore, we can approximately view m as fixed as n grows.

The conditional expectation and variance in Proposition 1 can be computed in $\mathcal{O}(m)$ time for each i when applying the Vecchia approximation to the covariance, resulting in a time complexity of $\mathcal{O}(nm)$ per MC sample.

PROPOSITION 2. Suppose $\mathbf{x} \sim \phi_n(\mathbf{x}; \Sigma)$, where Σ is the covariance matrix under the Vecchia approximation defined by the conditioning sets $\{c(i)\}_{i=1}^n$. Then,

$$\begin{aligned}\eta_i &:= E[x_i | \mathbf{x}_{1:i-1}] = \mathbf{A}_{i,:} \mathbf{x}, \\ l_i^2 &:= \text{Var}[x_i | \mathbf{x}_{1:i-1}] = \mathbf{V}_{i,i}^{-2},\end{aligned}$$

where \mathbf{A} is a sparse matrix $\mathbf{A}^\top = (\text{diag}(\mathbf{1}) - \mathbf{V}) \cdot \text{diag}(\mathbf{1})^{-1}$, \mathbf{V} is the (sparse) inverse Cholesky factor of Σ , $\Sigma = (\mathbf{V}\mathbf{V}^\top)^{-1}$, and $\mathbf{1}$ is the inverse of the diagonal entries of \mathbf{V} .

This definition of \mathbf{l} coincides with that above, namely the univariate conditional standard deviations. With the above expressions for the conditional mean and standard deviation, we can now transform the SOV and MET algorithms such that MC sampling can be performed at linear complexity.

3.2 Transforming SOV and MET

Algorithm 1 describes the MC sampling stage of our transformed Vecchia MET (VMET) based on the sparse matrix \mathbf{A} and the conditional standard deviation \mathbf{l} . The exponential tilting parameter γ can be obtained as discussed in Section 4 during the pre-processing stage, or it can be set as $\gamma = \mathbf{0}$ to obtain Vecchia SOV (VSOV) as a special case. Here, we use \mathbf{w} to denote a sample from the unit

Algorithm 1: Vecchia MET integrand

Input: $\mathbf{a}, \mathbf{b}, \mathbf{A}, \mathbf{l}, \gamma, \mathbf{w}$

Result: One sample of the MET integrand and (optionally) the proposal distribution

```

1: Initialize  $\mathbf{x} \leftarrow \mathbf{0}, h \leftarrow 1$ 
2: for  $i = 1, 2, \dots, n$  do
3:   if  $i > 1$  then
4:      $\mu_i \leftarrow \mathbf{A}_{i,:} \mathbf{x}$ 
5:   else
6:      $\mu_i \leftarrow 0$ 
7:   end if
8:    $\tilde{a}_i \leftarrow \frac{a_i - \mu_i}{l_i} - \gamma_i, \tilde{b}_i \leftarrow \frac{b_i - \mu_i}{l_i} - \gamma_i, p_i \leftarrow \Phi(\tilde{b}_i) - \Phi(\tilde{a}_i)$ 
9:    $y_i \leftarrow \Phi^{-1}(w_{i-1} \cdot p_i + \Phi(\tilde{a}_i)) + \gamma_i, x_i \leftarrow \mu_i + y_i \cdot l_i$ 
10:   $h \leftarrow h \cdot p_i \cdot \phi(y_i) / \phi(y_i - \gamma_i)$ 
11: end for
12: if Sampling from TMVN then
13:   return  $h$  and  $\mathbf{x}$ 
14: else
15:   return  $h$ 
16: end if
```

hypercube in \mathbb{R}^n , offering users the flexibility of choosing different MC rules. Compared to MET, the complexity of each iteration (i.e., for each i) is reduced from $\mathcal{O}(n)$ to $\mathcal{O}(m)$ employing the sparsity of \mathbf{A} in Step 4. Therefore, the per-sample complexity is reduced from $\mathcal{O}(n^2)$ to $\mathcal{O}(n)$ during the MC sampling stage. We refer to Algorithm 1 as ‘integrand’ to distinguish from ‘method’,

which includes both pre-processing and MC sampling. Algorithm 1 can be also used for accept-reject sampling of TMVN distributions, where \mathbf{x} is a sample generated from the proposal density $q(\mathbf{x})$ in (4) and h is the PDF ratio in (5). VMET allows us to fully exploit the sparseness of \mathbf{V} by using the original integration variable \mathbf{x} , whereas MET uses the transformed $\mathbf{y} = \mathbf{L}^{-1}\mathbf{x}$. Since the Vecchia approximation amounts to a valid MVN density with (slightly) different covariance, Algorithm 1 enjoys the same analytical properties and efficacy in the variance reduction of the integrand samples as the original MET integrand (Botev, 2017). This is supported by our theoretical and numerical results in Sections 4 and 6, respectively.

4 Solving For Exponential Tilting Parameters

Botev (2017) proposed to find the optimal γ , denoted by $\hat{\gamma}$, by minimizing the worst likelihood ratio as shown in (6). Denoting $\log h$ by ψ , Botev (2017) showed that ψ is convex with respect to (w.r.t.) γ and concave w.r.t. \mathbf{y} . Hence, finding $\hat{\gamma}$ amounts to finding the solution $(\hat{\mathbf{y}}, \hat{\gamma})$ of the nonlinear system $\nabla\psi = \mathbf{0}$ if the solution satisfies $\mathbf{a} \leq \mathbf{L}\hat{\mathbf{y}} \leq \mathbf{b}$, which was empirically shown to be true by Botev (2017). Under our parameterization of ψ that uses \mathbf{x} instead of \mathbf{y} , it can be shown that the convex-concave property still holds.

PROPOSITION 3. *For fixed \mathbf{x} , ψ is a convex function of γ ; for fixed γ , ψ is a concave function of \mathbf{x} . Therefore,*

$$\hat{\gamma} = \arg \min_{\gamma} \max_{\mathbf{a} \leq \mathbf{x} \leq \mathbf{b}} \psi(\mathbf{x}; \gamma)$$

is a saddle point problem with a unique solution given by $\nabla\psi(\mathbf{x}; \gamma) = \mathbf{0}$.

However, solving $\nabla\psi = \mathbf{0}$ amounts to finding the solution of a challenging non-linear system of $2n$ variables. Botev (2017) used the trust-region method described in Powell (1970), which minimizes $g := \|\nabla\psi\|^2$ through building a quadratic approximation of g at the current values of (\mathbf{y}, γ) . Notice that Botev (2017) viewed ψ , hence g , as functions of (\mathbf{y}, γ) where as we view them as functions of (\mathbf{x}, γ) . The quadratic approximation of g requires the computation of $\mathbf{H} \cdot \nabla\psi$ and $\mathbf{H}^{-1} \cdot \nabla\psi$, where \mathbf{H} denotes the Hessian matrix of ψ . This involves expensive $\mathcal{O}(n^3)$ matrix operations, and empirically the computational cost for solving $\nabla\psi = \mathbf{0}$ exceeds that for MC sampling when $n \sim 10^3$, rendering MET significantly slower than SOV and other methods.

In Proposition 4, we derive $\nabla\psi$ and \mathbf{H} under the parameterization of ψ that uses \mathbf{x} , \mathbf{A} and \mathbf{I} . Utilizing the sparse-matrix representation of \mathbf{H} , we propose an $\mathcal{O}(n)$ gradient-based method for solving $\hat{\gamma}$ that proves to be significantly more efficient than and as effective as using the trust-region method in Botev (2017).

PROPOSITION 4. *Denote the logarithm of the density ratio, $\log h(\mathbf{x}; \gamma)$, from (5) by ψ . Under the Vecchia approximation, the gradient and Hessian of ψ can be derived as:*

$$\frac{\partial\psi}{\partial\mathbf{x}} = -(\mathbf{I} - \mathbf{A})^\top \mathbf{D}_1^{-1} \gamma + \mathbf{A}^\top \mathbf{D}_1^{-1} \Psi, \quad \frac{\partial\psi}{\partial\gamma} = \gamma - \mathbf{D}_1^{-1}(\mathbf{x} - \boldsymbol{\mu}_c) + \Psi, \quad (7)$$

$$\mathbf{H} = \begin{bmatrix} \mathbf{A}^\top \mathbf{D}_1^{-1} \Psi' \mathbf{D}_1^{-1} \mathbf{A} & -(\mathbf{I} - \mathbf{A})^\top \mathbf{D}_1^{-1} + \mathbf{A}^\top \mathbf{D}_1^{-1} \Psi' \\ -\mathbf{D}_1^{-1}(\mathbf{I} - \mathbf{A}) + \mathbf{D}_1^{-1} \Psi' \mathbf{A} & \mathbf{I} + \Psi' \end{bmatrix}, \quad (8)$$

where \mathbf{D}_1 is the $n \times n$ diagonal matrix with diagonal entries equal to 1, Ψ is a vector of length n with i th entry

$$\Psi_i = \frac{\phi(\tilde{a}_i; \gamma_i, 1) - \phi(\tilde{b}_i; \gamma_i, 1)}{\Phi(\tilde{b}_i - \gamma_i) - \Phi(\tilde{a}_i - \gamma_i)},$$

and Ψ' is a $n \times n$ diagonal matrix with i th diagonal entry

$$\Psi'_{i,i} = \frac{(\tilde{a}_i - \gamma_i)\phi(\tilde{a}_i; \gamma_i, 1) - (\tilde{b}_i - \gamma_i)\phi(\tilde{b}_i; \gamma_i, 1)}{\Phi(\tilde{b}_i - \gamma_i) - \Phi(\tilde{a}_i - \gamma_i)} - \Psi_i^2,$$

with $\tilde{\mathbf{a}} = \mathbf{D}_1^{-1}(\mathbf{a} - \mathbf{A}\mathbf{x})$ and $\tilde{\mathbf{b}} = \mathbf{D}_1^{-1}(\mathbf{b} - \mathbf{A}\mathbf{x})$.

Based on these expressions, we propose to minimize g for VMET using a gradient-based optimizer, for which $\nabla g = \mathbf{H} \cdot \nabla \psi$ can be computed efficiently in $\mathcal{O}(n)$ time, and which does not require the more expensive $\mathbf{H}^{-1} \cdot \nabla \psi$. Specifically, due to the sparsity of \mathbf{A} with fewer than nm non-zero coefficients, $\nabla \psi$ in (7) and matrix-vector products involving \mathbf{H} can be computed in $\mathcal{O}(nm)$ time. In our implementation, we use the Broyden-Fletcher-Goldfarb-Shanno (L-BFGS) algorithm (Liu and Nocedal, 1989) as our optimizer, which creates a low-rank approximation of the Hessian of g , maintaining an overall $\mathcal{O}(n)$ complexity. Another advantage of VMET over MET is that the Hessian of ψ with respect to \mathbf{x} , $\frac{\partial^2 \psi}{\partial \mathbf{x}^2}$, can be represented using the sparse matrix \mathbf{A} , and so $\arg \max_{\mathbf{x}} \psi(\mathbf{x}; \gamma)$ can be solved efficiently with second-order optimization algorithms. Finding $\max_{\mathbf{x}} \psi(\mathbf{x}; \gamma)$, which is the logarithm of the maximum PDF ratio (i.e., $\max \log h$ in (5)), accurately for a given γ is crucial to the accept-reject sampling of TMVN distributions introduced in Section 2.

An important property of the MET integrand is the vanishing relative error property (VRE) that was proved in Botev (2017) based on the minimax definition of $\hat{\gamma}$. The VRE property can also be proved for our proposed VMET integrand.

PROPOSITION 5. *The integrand $h(\mathbf{x}; \hat{\gamma}) = \exp \psi(\mathbf{x}; \hat{\gamma})$ has vanishing relative error. That is*

$$\limsup_{\gamma \rightarrow +\infty} \frac{\text{var}(h(\mathbf{x}; \hat{\gamma}))}{h^2(\mathbf{x}; \hat{\gamma})} = 0,$$

when the integration limits are $(\gamma \mathbf{a}, +\infty)$ and $a_i > 0$ for $i = 1, \dots, n$. Here, the variance is taken with respect to \mathbf{x} sampled from $q(\mathbf{x}; \hat{\gamma})$.

The VRE property suggests that the proposal density $q(\mathbf{x}; \hat{\gamma})$ can become indistinguishable from the MVN density $\phi_n(\mathbf{x}; \Sigma)$ truncated in the region of $(\gamma \mathbf{a}, +\infty)$.

5 Variable Reordering Based on Vecchia

An integration-variable reordering method, referred to as univariate variable reordering, based on the correlation structure in Σ and the integration limits \mathbf{a} and \mathbf{b} was described in Genz and Bretz (2009) to empirically improve the MC sampling variance. Univariate reordering, which is provided in Algorithm 2, iteratively computes conditional univariate normal probabilities and prioritizes the one with the smallest probability, resulting in $\mathcal{O}(n^3)$ complexity.

We propose a fast Vecchia-based version of the univariate variable reordering in Algorithm 3. Under the Vecchia approximation, the conditional expectation and variance in Line 6 of Algo-

Algorithm 2: Univariate variable reordering (Genz and Bretz, 2009)

Input: $n, \mathbf{a}, \mathbf{b}, \Sigma$ **Result:** New variable order \mathbf{r}

- 1: Initialize $\mathbf{r} \leftarrow [1, \dots, n]$, $\boldsymbol{\sigma} \leftarrow \text{diag}(\Sigma)^{1/2}$, $\boldsymbol{\mu} \leftarrow \mathbf{0}_n$
 - 2: **for** $i = 1, 2, \dots, n$ **do**
 - 3: $j \leftarrow \arg \min_{j \geq i} \Phi((b_j - \mu_j)/\sigma_j) - \Phi((a_j - \mu_j)/\sigma_j)$
 - 4: Switch the i -th and j -th coefficient in $\mathbf{a}, \mathbf{b}, \boldsymbol{\sigma}, \boldsymbol{\mu}$, and \mathbf{r}
 - 5: Compute $E_{X \sim N(\mu_i, \sigma_i)}[X \mid a_i < X < b_i]$ and assign to μ_i
 - 6: Under $\mathbf{x} \sim N_n(\mathbf{0}, \Sigma)$, compute $\mu_j \leftarrow E[x_j \mid \mathbf{x}_{1:i} = \boldsymbol{\mu}_{1:i}]$
 $\sigma_j \leftarrow \sqrt{\text{Var}[x_j \mid \mathbf{x}_{1:i} = \boldsymbol{\mu}_{1:i}]}$, for $j = i + 1, \dots, n$
 - 7: **end for**
 - 8: **return** \mathbf{r}
-

Algorithm 3: Vecchia-based variable reordering

Input: $n, \mathbf{a}, \mathbf{b}, \Sigma$ **Result:** New variable order \mathbf{r}

- 1: Standardize $\mathbf{a}, \mathbf{b}, \Sigma$ s.t. $\text{diag}(\Sigma) = \mathbf{1}$
 - 2: Initialize $\mathbf{r} \leftarrow [1, \dots, n]$, $\boldsymbol{\sigma} \leftarrow \text{diag}(\Sigma)^{1/2}$, $\boldsymbol{\mu} \leftarrow \mathbf{0}_n$, $c(j) \leftarrow \{\}$ for $j = 1, \dots, n$
 - 3: **for** $i = 1, 2, \dots, n$ **do**
 - 4: $j \leftarrow \arg \min_{j \geq i} \Phi((b_j - \mu_j)/\sigma_j) - \Phi((a_j - \mu_j)/\sigma_j)$
 - 5: Switch the i -th and j -th coefficient in $\mathbf{a}, \mathbf{b}, \boldsymbol{\sigma}, \boldsymbol{\mu}$, and \mathbf{r}
 - 6: Compute $E[X \mid X \sim N(\mu_i, \sigma_i), a_i < X < b_i]$ and assign to μ_i
 - 7: **for** $j = i + 1, \dots, n$ **do**
 - 8: **if** $|c(j)| < m$ **or** $\min(\Sigma_{s_j, s_{c(j)}}) < \Sigma_{s_j, s_i}$ **then**
 - 9: $c(j) \leftarrow c(j) \cup \{i\}$
 - 10: **if** $|c(j)| > m$ **then**
 - 11: $k \leftarrow \arg \min \Sigma_{s_j, s_{c(j)}}$, remove the k -th coefficient in $c(j)$
 - 12: **end if**
 - 13: $\mu_j \leftarrow E[x_j \mid \mathbf{x}_{c(j)} = \boldsymbol{\mu}_{c(j)}]$, $\sigma_j \leftarrow \sqrt{\text{Var}[x_j \mid \mathbf{x}_{c(j)} = \boldsymbol{\mu}_{c(j)}]}$
 - 14: **end if**
 - 15: **end for**
 - 16: **end for**
 - 17: **return** \mathbf{r}
-

rithm 2 can be computed in $\mathcal{O}(m^3)$ time for each j as indicated by Line 13 of Algorithm 3, amounting to a total algorithm complexity of $\mathcal{O}(n^2)$. Because the conditioning sets in the Vecchia approximation are subsets of previous indices (i.e., $c(i) \subset \{1, \dots, i-1\}$), we need to construct and update the conditioning sets during univariate reordering as described in Lines 9 and 11 of Algorithm 3, where the conditioning sets are chosen as the m previously indexed integration variables that have the strongest correlation with the j -th integration variable.

Variable reordering can be reduced to linear complexity under a special case of the Vecchia approximation with $c(i) = \{1, \dots, m\}$ for $i > m$, which results in the fully independent conditional (FIC) approach (Katzfuss and Guinness, 2021; Snelson and Ghahramani, 2007), one of

the most popular GP approximations in machine learning. Under the FIC assumption, the variable ordering (after selecting the first m variables) can be obtained in a single iteration, hence achieving an overall $\mathcal{O}(n)$ complexity. For the first m variables, we can simply run the loop in Algorithm 2 for m iterations. We refer to this $\mathcal{O}(n)$ ordering as the FIC-based variable reordering to distinguish it from the $\mathcal{O}(n^2)$ Vecchia-based variable reordering in Algorithm 3. We provide a numerical comparison on the classic univariate reordering, the Vecchia-based variable reordering, and the FIC-based variable reordering in Section 6.1.

Algorithm 4 summarizes our proposed method for estimating MVN probabilities and sampling TMVN distributions by combining the results from Sections 3 and 4 with the variable reordering introduced in this section. In most settings, Σ is a kernel matrix that does not need to be stored

Algorithm 4: The VMET method

Input: $n, \mathbf{a}, \mathbf{b}, \Sigma, N$

Result: MVN probability estimate **OR** samples from a TMVN distribution

- 1: **if** Reordering needed **then**
 - 2: $\mathbf{r} \leftarrow$ Algorithm 3($n, \mathbf{a}, \mathbf{b}, \Sigma$), $\mathbf{a} \leftarrow \mathbf{a}[\mathbf{r}]$, $\mathbf{b} \leftarrow \mathbf{a}[\mathbf{r}]$, $\Sigma \leftarrow \Sigma[\mathbf{r}, \mathbf{r}]$
 - 3: **end if**
 - 4: Compute \mathbf{A} and \mathbf{l} defined in Section 3.1 with Σ
 - 5: Minimize (e.g., using L-BFGS) $g = \|\nabla\psi\|^2$ described in (7) with $\nabla g = \mathbf{H} \cdot \nabla\psi$ described in (7) and (8). Denote the solution by $(\hat{\mathbf{x}}, \hat{\gamma})^\top$
 - 6: **for** $i = 1, \dots, N$ **do**
 - 7: Draw \mathbf{w} from the unit hypercube. Run Algorithm 1($\mathbf{a}, \mathbf{b}, \mathbf{A}, \mathbf{l}, \gamma, \mathbf{w}$)
 - 8: **if** Samples from a TMVN distribution is needed **then**
 - 9: Generate $U \sim \text{uniform}(0, 1)$, if $U \exp \psi(\hat{\mathbf{x}}, \hat{\gamma}) < p$, accept \mathbf{x} , reject otherwise
 - 10: **else**
 - 11: Record $p_i = p$. The average of $\{p_i\}$ is the estimate of $\Phi_n(\mathbf{a}, \mathbf{b}, \Sigma)$
 - 12: **end if**
 - 13: **end for**
-

explicitly and whose entries can be computed as needed based on the kernel and the relevant inputs or locations, resulting in a $\mathcal{O}(n)$ memory footprint. After variable reordering, VMET has a time complexity of $\mathcal{O}(Tnm + Nnm)$, where the summands correspond to optimizing the exponential tilting parameter γ and drawing MC samples of the VMET integrand. The number of iterations T for optimizing γ typically ranges between 500 and 1,000, while the MC sample size N is typically between 10^4 and 10^5 . Although the Vecchia-based variable reordering has a quadratic complexity in n , it has a lower computation cost than MC sampling in practice, where typically $N > n$. For estimating unknown parameters in Σ , we do not carry out variable reordering to achieve a smooth likelihood that is beneficial to optimization, as will be discussed in Section 7.1.

6 Numerical comparison

In this section, we first show that integration variable reordering has a significant impact on the variance of the MET and VMET integrand samples when evaluating MVN probabilities with spatial covariance matrices. Next, we compare the following methods:

VMET: our proposed Vecchia-based method, summarized in Algorithm 4

SOV: the SOV method from Genz (1992); Genz and Bretz (2009)

MET: the MET method from Botev (2017)

TLR: the TLR SOV method from Cao et al. (2021)

VCDF: the Vecchia approximation of MVN CDFs from Nascimento and Shaby (2022)

The original implementation of SOV in the R package `mvtnorm` (Genz and Bretz, 2009) only allows input MVN dimensions n up to 1,000; for $n > 1,000$ we used the SOV implementation in `tlrmvnmvt` (Cao et al., 2022a). The implementations used for MET, TLR, and VCDF were the `TruncatedNormal` (Botev, 2017) R package, the `tlrmvnmvt` (Cao et al., 2022a) R package, and the R package from <https://github.com/Recca2012/CDFApprox>, respectively. Computation times were measured on Intel Xeon E5-2680 v4 CPU.

6.1 Variable reordering comparison

In this section, we show that the variable reordering heuristic proposed for SOV (Genz and Bretz, 2009) can also improve the results for MET and VMET. We demonstrate that our proposed Vecchia-based variable reordering (Algorithm 3) can achieve the same level of improvement in reducing the MC variance as the univariate reordering (Algorithm 2). SOV and TLR are not considered in this section, because their benefits from variable reordering have been documented in the literature (e.g., Cao et al., 2022a; Genz and Bretz, 2009).

We considered three low-dimensional ($n = 900$) MVN probabilities to allow comparisons to the non-scalable MET method as a gold standard. All three examples used a Matérn-1.5 kernel in \mathbb{R}^2 with variance 1, range 0.1, and nugget variance 0.01. The three scenarios, which are summarized in Table 1, cover a variety of settings, including regular versus irregular locations, same versus different integration intervals, and tail versus centered probabilities.

| | spatial locations $\{\mathbf{s}_i\}_{i=1}^n$ | lower limits \mathbf{a} | upper limits \mathbf{b} |
|------------|--|---------------------------|---------------------------|
| Scenario 1 | grid in $[0, 1]^2$ | $-\infty$ | $\mathbf{0}$ |
| Scenario 2 | Latin hypercube in $[0, 1]^2$ | $-\infty$ | Uniform($-2, 0$) |
| Scenario 3 | grid in $[0, 1]^2$ | $-\mathbf{1}$ | $\mathbf{1}$ |

Table 1: Spatial locations and integration limits for three simulation scenarios. Uniform($-2, 0$) refers to generating random numbers from the uniform distribution in $(-2, 0)$ independently for each coefficient.

Figure 1 compares the MET and VMET (with $m = 30$) integrands with and without univariate variable reordering, where each boxplot consists of thirty estimates and each estimate used $N = 10,000$ MC samples. Variable reordering reduced the variability of both integrands, hence improving the accuracy for MVN probability estimation. The effectiveness of variable reordering varied across different MVN probabilities. In Scenario 3, where integration limits were centered and the same across integration variables, variable reordering had a smaller impact than in the other two cases. Furthermore, our proposed VMET integrand had overall negligible bias and the same level of variability compared with the MET integrand.

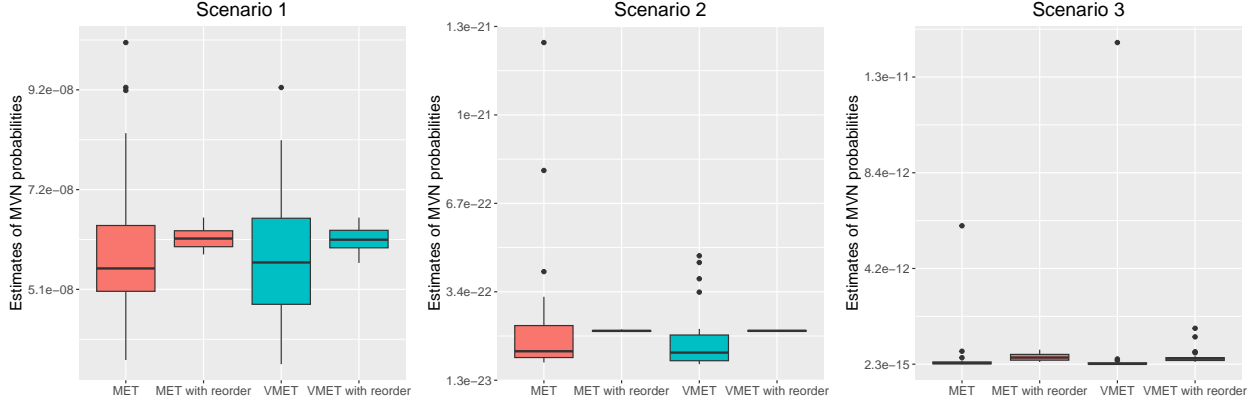


Figure 1: Impact of variable reordering on MET and VMET integrands for the three scenarios described in Table 1. Each boxplot consists of 30 estimates of the same MVN probability.

Figure 2 compares the VMET integrand based on four different reordering approaches: no reordering, FIC-based reordering (last paragraph of Section 5), Vecchia-based reordering, and classic univariate reordering. We used conditioning-set size $m = 30$ for Vecchia and $m = 30, 100, 200$

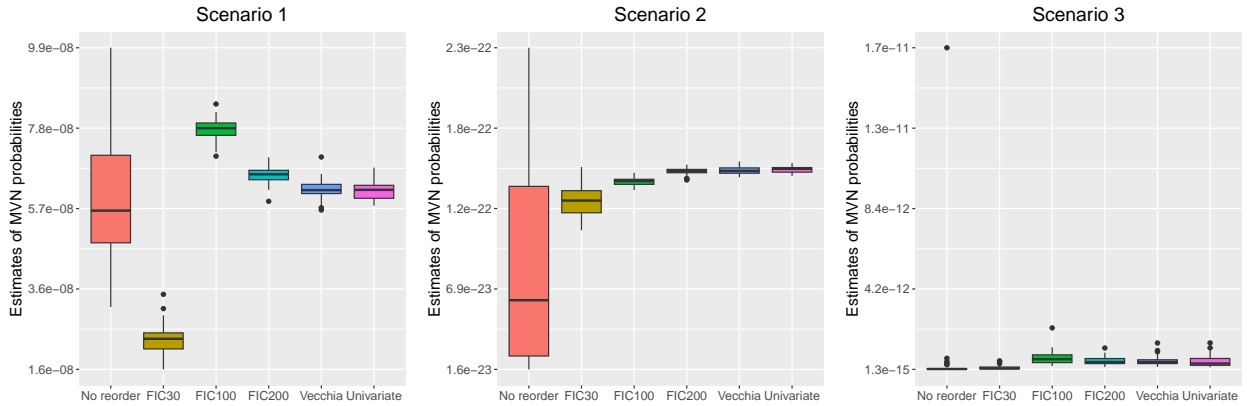


Figure 2: Comparison of FIC-based variable reordering ($m = 30$ and $m = 100$), Vecchia-based variable reordering ($m = 30$), and univariate reordering for the three scenarios described in Table 1. Each boxplot consists of 30 estimates using the VMET integrand.

for FIC to showcase the convergence of the FIC-based variable reordering to the Vecchia based variable reordering. The improvement from the FIC-based reordering depended on the experiment scenario and the choice of m , but FIC-based reordering already achieved significant variance reduction with $m = 100$ and similar level of variance reduction as Vecchia-based and univariate reorderings with $m = 200$. Furthermore, when the FIC approximation has been applied to the underlying GP, the FIC-based reordering will produce the same ordering as the univariate reordering. Vecchia-based reordering and univariate reordering were almost identical in MC variance reduction, both more effective than the FIC-based reordering with $m \leq 100$. Our proposed Vecchia-based reordering reduces the computation cost by a factor of n compared to univariate reordering. In practice, the cost of variable reordering is typically much lower than that of MC sampling and solving for $\hat{\gamma}$. Henceforth, we use the Vecchia-based reordering preceding the VMET integrand and refer to the combination as the VMET method.

6.2 Comparison for low-dimensional MVN probabilities

We compared the methods listed at the beginning of Section 6 on the same three scenarios in Table 1 used in Section 6.1 with $n = 900$. The resulting log-probabilities and the computation times for the three MVN problems are plotted in Figure 3. The log scale was needed to accommodate the

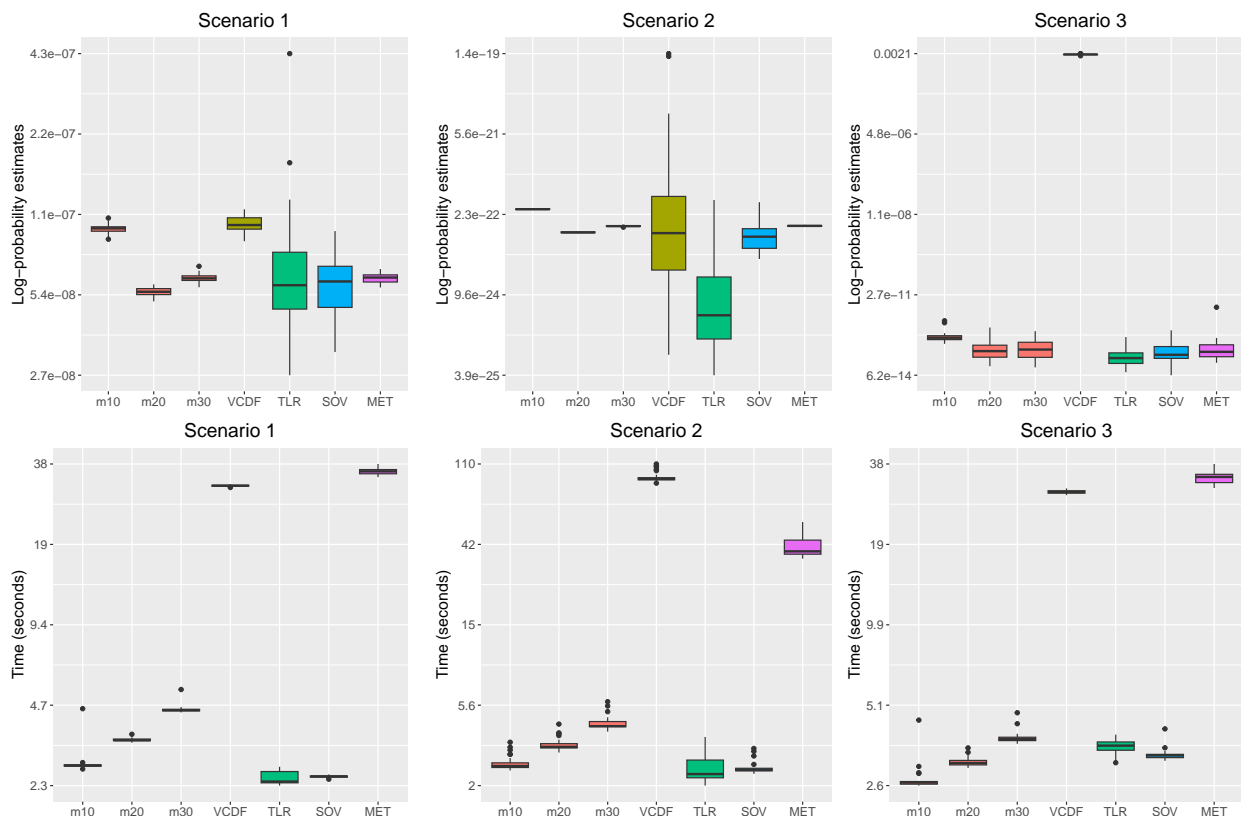


Figure 3: For the scenarios in Table 1 with $n = 900$, we show 30 log-probability estimates (top row) and computation times (bottom row) each for VMET, VCDF, TLR, SOV, and MET. VMET was run with $m = 10, 20, 30$. MET is the gold standard in terms of accuracy (but it is infeasible for large n).

substantially different accuracy levels of some of the methods. The true values of the three MVN probabilities are unknown, but the MET method can be considered the gold standard. (But note that MET is not computationally scalable to large n .) For our VMET method, we used $m = 10, 20, 30$ to demonstrate the trade-off between estimation bias and computation efficiency.

Overall, VCDF had the largest estimation errors (including bias and variance), especially in the third example. TLR slightly under-performed SOV in the first and third examples but produced significant estimation errors in the second example, which was likely due to the difference between univariate reordering and the block variable reordering used in TLR becoming more pronounced when the integration limits were very different across integration variables. Our method at $m = 30$ had negligible bias and similar variance compared to the gold-standard MET in all three scenarios, substantially outperforming all other scalable methods in terms of accuracy. The third example had centered integration limits, where the optimal $\hat{\gamma}$ for the proposal density used in MET and VMET was simply zero, hence the MET integrands were identical to the SOV integrands. For MET, solving for $\hat{\gamma}$ was already much more computationally expensive than the combination of

variable reordering and MC sampling when $n = 900$ and $N = 10,000$. Utilizing our proposed linear-complexity gradient and Hessian estimators in (7) and (8), the optimization cost of γ was reduced by more than 90% for $n = 900$. We show in the next section that due to our complexity advantage, which is $\mathcal{O}(n)$ and $\mathcal{O}(n^{0.5})$ lower than SOV and TLR, respectively, our computation times were lower than those of SOV and TLR when n was larger. The estimation bias of our method can be significant when m is chosen too small (e.g., $m = 10$ in Figure 3), but a reasonably large m (e.g., between 30 and 50) was sufficient to achieve negligible bias in our comparisons, even in tens of thousands of dimensions.

6.3 Comparison for high-dimensional MVN probabilities

For larger n , we only compared our method to TLR and SOV, as MET and VCDF are computationally infeasible. We considered three $n = 6,400$ -dimensional MVN probabilities according to Scenarios 1 to 3 in Table 1, respectively. For this high-dimensional study, the nugget parameter was increased from 0.01 to 0.03 to avoid singularity, while the other covariance parameters remained unchanged. As $m \leq 20$ resulted in bias in Section 6.2, we considered m between 30 and 50 for VMET. The log-probability estimates and computation times are shown in Figure 4; only one boxplot is included for computation times, as the three boxplots for computation times were almost identical.

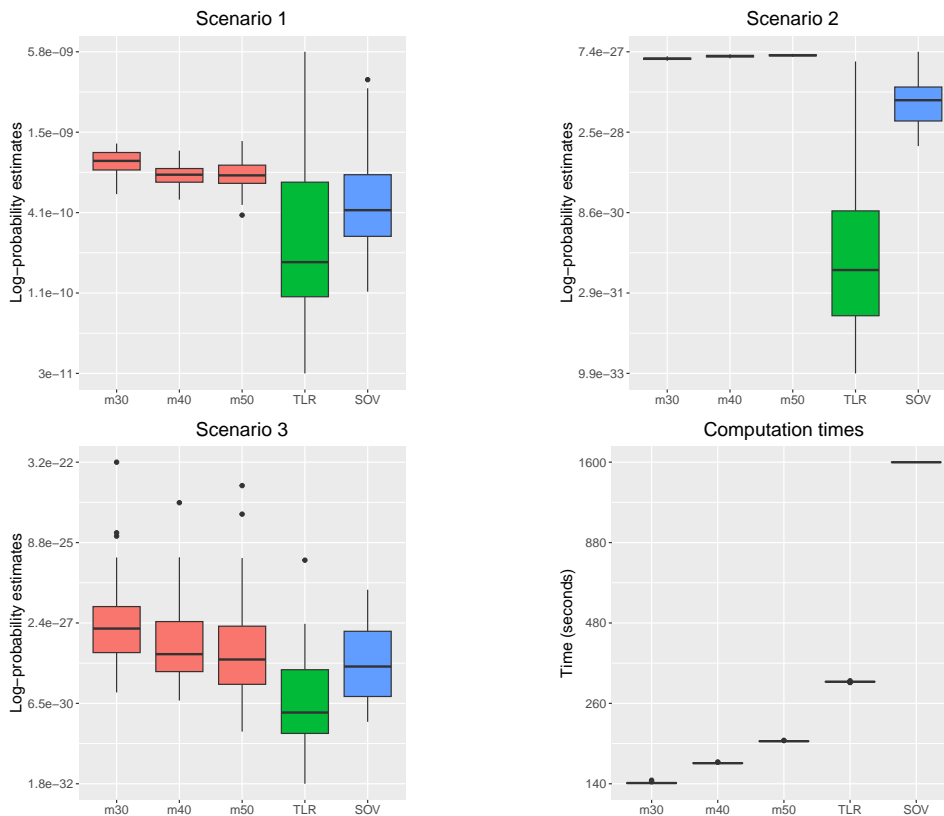


Figure 4: For the simulation scenarios in Table 1 with $n = 6,400$, thirty log-probability estimates for VMET, TLR, and SOV methods. The bottom right panel shows the computation times of the three methods, which was approximately the same for all three scenarios. VMET was run with $m = 30, 40$, and 50 .

For the high-dimensional experiments, we used $N = 10^5$ MC samples. For Scenarios 1 and 2, we considered VMET with $m = 50$ as the benchmark, as VMET arguably has lower MC variance than SOV and TLR for tail MVN probabilities and the bias caused by the Vecchia approximation was likely negligible. For Scenario 3, we used SOV as benchmark, because for centered MVN probabilities, MET and SOV amount to the same integrand, hence SOV is expected to have approximately the same level of MC variance as VMET but without bias. Compared with SOV, VMET significantly reduced the MC variance for tail MVN probabilities, while for centered MVN probabilities, both had almost the same MC variance. Scenario 2 appeared to suggest that TLR and SOV had estimation bias but the underestimation of TLR and SOV were due to their extremely low probability of sampling into the region where the integration mass is concentrated; in other words, optimizing γ according to (6) in VMET provided vast improvements over implicitly using $\gamma = 0$ in TLR and SOV. At $n = 6,400$, VMET with $m = 30$ displayed a small amount of bias, which was alleviated by a slight increase in m , for example to 40. The computation times of our proposed VMET were approximately half of those of TLR and less than $1/8$ of those of SOV, highlighting VMET’s complexity advantage over TLR and SOV. Overall, our proposed VMET method outperformed SOV and TLR in terms of both the MC variance of the integrand samples and in terms of computational scalability. Furthermore, TLR, the currently most scalable method, may suffer from unpredictable numerical singularity, whereas VMET is more numerically stable, because unlike low-rank matrix approximations, the Vecchia approximation has the theoretical guarantee of maintaining positive definiteness.

6.4 Sampling from TMVN distributions

Our proposed VMET method can also be used for sampling from TMVN distributions. We compared the performance of VMET with that of MET in terms of the quantile-quantile (q-q) plot of the drawn samples and the time used. For the TMVN distribution, we considered Scenario 1 in Table 1 with $n = 900$ and the same Matérn kernel as in Sections 6.1 and 6.2. We generated $N = 1,000$ samples using the VMET method with $m = 30$ described in Algorithm 1 and the MET method implemented in the `TruncatedNormal` R package; a visual comparison is provided in Figure 5.

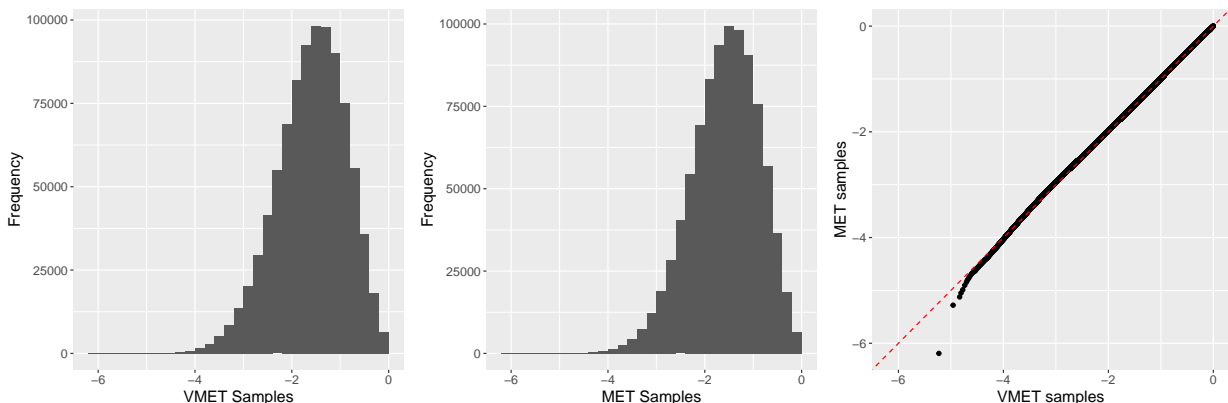


Figure 5: Histograms and q-q plot of the TMVN samples generated by our proposed VMET method and the MET method (Botev, 2017)

The two groups of samples aligned very well with each other except for the very tail region, because VMET essentially truncates the conditioning set compared with MET, which in this example pulled the conditional means towards the untruncated mean of zero. In terms of computation time, MET used 494.4 seconds, whereas VMET only used 19.9 seconds. The time difference will become even more pronounced for larger n .

Note that the acceptance rate can be too low to draw exact samples from the TMVN distribution for moderately large n , for example 10^3 , even with the exponential tilting proposal density (4). Hence, for large n , we propose a regional sampling technique in Section 7 for drawing samples only over a region of interest.

7 Analysis of Partially Censored Data

Censoring is a common issue in many application areas including environmental science, where sensors in earth, water, or air often have a threshold below which the quantity of interest cannot be detected. Assuming that the quantity of interest follows a joint normal distribution, the observed and censored data collected by the sensor jointly follow a censored MVN distribution. Mathematically, assuming a zero mean, the data $\mathbf{z} = [z_1, \dots, z_n]^\top$ follow a censored MVN distribution if

$$\mathbf{x} \sim \mathcal{N}(\mathbf{0}, \Sigma), \quad z_i = \begin{cases} x_i, & \text{if } x_i > b_i, \\ \text{NA}, & \text{otherwise,} \end{cases}$$

where \mathbf{x} is the quantity of interest that the sensors are attempting to measure, and $\{b_i\}$ are detection thresholds of the sensors. Without loss of generality, we assume that only the first n_1 locations are observed (i.e., $x_i > b_i$ if and only if $i \leq n_1$).

Given the data \mathbf{z} , the likelihood of the censored MVN distribution is:

$$f(\mathbf{z}) = f_{\mathbf{x}_{1:n_1}}(\mathbf{z}_{1:n_1}) \Pr(\mathbf{x}_{n_1+1:n} < \mathbf{b}_{n_1+1:n} \mid \mathbf{x}_{1:n_1} = \mathbf{z}_{1:n_1}).$$

Under the Vecchia approximation, the above likelihood can be written as

$$f(\mathbf{z}) = \left(\prod_{i=1}^{n_1} f(x_i \mid \mathbf{x}_{c(i)}) \right) \left(\int_{-\infty}^{\mathbf{b}_{n_1+1:n}} \prod_{i=n_1+1}^n f(x_i \mid \mathbf{x}_{c(i)}) d\mathbf{x}_{n_1+1:n} \right). \quad (9)$$

Notice that $\mathbf{x}_{c(i)}$ for $i > n_1$ may include observed x_j (i.e., with $j \leq n_1$). We can view (9) as a limit case of the general MVN probability in (1) with $\mathbf{a}_{1:n_1} \rightarrow \mathbf{z}_{1:n_1} \leftarrow \mathbf{b}_{1:n_1}$ and $\mathbf{a}_{n_1+1:n} = -\infty$.

7.1 Parameter estimation

It is common practice in many environmental applications to substitute censored data with a constant value, such as half the level of detection (LOD), the LOD divided by the square root of 2, or simply zero (Croghan and Egeghy, 2003). These LOD-based methods are also broadly used as a benchmark for more sophisticated Markov-chain-Monte-Carlo-based methods (De Oliveira, 2005; Ordoñez et al., 2018; Schelin and Sjöstedt-de Luna, 2014), which are often not scalable to large n . We show that in the presence of censored data, the censored MVN model in (9) can achieve more

accurate parameter estimation than LOD-based methods. We generated a spatial field \mathbf{x} over 6,400 locations on a 80×80 grid in the unit square based on a GP with mean zero and a Matérn covariance with variance, range, smoothness, and nugget of $(1.0, 0.1, 1.5, 0.03)$ in the same setup as Scenario 1 in Table 1. All x_i values below $b_i = 0$ were censored to obtain the data \mathbf{z} . Because the censoring thresholds were zero, all LOD-based methods discussed in (Croghan and Egeghy, 2003) amounted to the same data augmentation. We considered a specific realization, for which 2,585

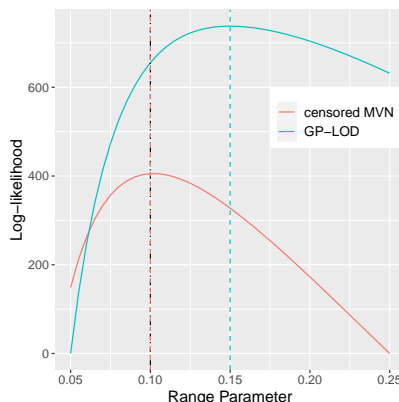


Figure 6: Log-likelihood curves as a function of the range parameter for our censored MVN approach and for the LOD-augmented GP. Both curves were vertically shifted to have their minimums at zero.

responses were censored and 3,815 were observed. To visualize the log-likelihood manifolds of the censored MVN model and the LOD approach, we fixed variance, smoothness, and nugget to their true values while plotting the log-likelihood against the range parameter. The GP log-likelihood using LOD-augmented data peaked at the range value of 0.15, whereas the censored MVN yielded a log-likelihood curve that peaked at exactly the true value 0.1, indicating the efficacy gain from properly including the information at censored locations. The parameter estimation performance differed more when the censoring threshold became higher (e.g., we tried $b_i = 1$), with censored MVN more significantly outperforming the LOD approach. For parameter estimation, we did not apply the variable reordering discussed in Section 5, as it would create discontinuity in the log-likelihood surface, limiting the potential for utilizing gradient-based optimizers.

7.2 Sampling TMVN over regions of interest

Once parameters have been estimated, we can sample the censored data given the observed data as in Section 6.4, holding the first n_1 observed data fixed. Unlike for parameter estimation, we recommend using the Vecchia-based variable reordering for sampling TMVN distributions to improve the acceptance rate. However, the acceptance rate for sampling the TMVN distribution can be very low even with exponential tilting when the number of censored responses is high (e.g., $(n - n_1) > 1,000$), making it infeasible to obtain a reasonable number of samples for posterior inference. In this case, we propose to divide the censored locations according to subregions of the input space, each containing a manageable number (say, at most 1,000) of censored locations; then we can draw separate TMVN samples over each region of interest conditioning on all observed responses but only on the censored responses in the same subregion. This idea is intuitive and simple to implement. Its downside is that it ignores censored locations not in the selected region.

As a heuristic remedy, we extend the boundary of the region of interest when drawing TMVN samples to incorporate surrounding information. In many applications, obtaining the joint posterior distribution of the quantity of interest over a subregion is sufficient; for example, one could obtain the joint distribution of a water-related quantity over a catchment area and then compute the distribution of functions of interests (e.g., the average) as necessary.

To demonstrate this idea, we first considered an example in sufficiently low dimensions so that the ‘global’ simulation of all censored locations had a reasonable acceptance rate above 10^{-4} . Specifically, we considered Scenario 1 in Table 1, where the censoring threshold is zero. Figure 7 compares $N = 1,000$ samples of the north-west quarter (i.e., $[0, 0.5] \times [0.5, 1.0]$) generated by the global and regional sampling schemes using VMET. For the regional sampling scheme, we

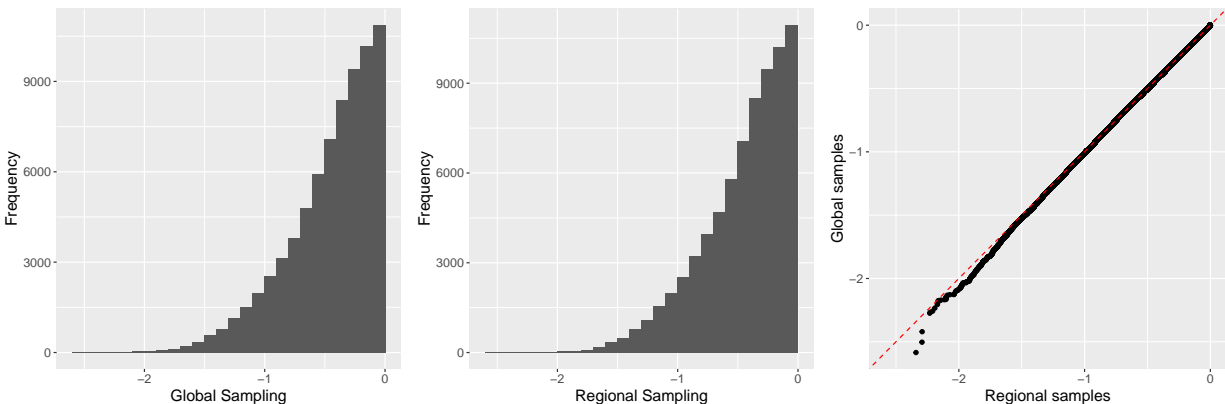


Figure 7: Histograms and q-q plot of the TMVN samples drawn by the ‘global’ and ‘regional’ schemes

sampled the TMVN distribution defined over the region $[0, 0.6] \times [0.4, 1.0]$, which enveloped the region of our interest, conditional on all observed locations. For the global sampling scheme, we needed to sample from a 380-dimensional TMVN distribution, whereas for the regional scheme, we only needed to sample from a 125-dimensional TMVN distribution, resulting in a 50 to 100 times difference in acceptance rates. The two groups of samples were very similar except for minor differences in the tails, which can be attributed to the reduced number of censored locations used in the regional sampling scheme. Conditioning on more censored locations would decrease the conditional mean under our Matérn covariance kernel. We also compared the RMSE for predicting the censored data in the north-west quarter, where the global and regional sampling produced errors of 0.24 and 0.25, respectively. In contrast, the GP with the LOD-augmented data produced a prediction error of 0.62 and the stochastic approximation of expectation maximization (SAEM), a state-of-the-art method for sampling TMVN distributions from Ordoñez et al. (2018), produced an error of 0.47. For SAEM, we set the MC sample size to 500 as in Ordoñez et al. (2018), resulting in a computation time of approximately two hours, which was significantly higher than for our proposed methods. The regional scheme had much higher accuracy than the competing methods and the minor accuracy loss compared with the global scheme, we believe, is a good trade-off for the gain in computational efficiency.

Next, we considered an example in higher dimensions to demonstrate that the VMET method can be used in combination with the regional sampling scheme to improve posterior inference when there are censored GP responses. We again considered Scenario 1 from Table 1, but now with $n = 6,400$. The region of interest and the region over which we drew TMVN samples were the

same as in the low-dimensional example above. We had a total of 3,278 censored locations, with 1,075 inside our sampling region. $N = 1,000$ samples were drawn and used in combination with all observed responses to predict the responses at 500 randomly selected testing locations in our region of interest (i.e., $[0, 0.5] \times [0.5, 1.0]$). For comparison, we predicted with the GP using the LOD-augmented data; we also attempted a comparison to SAEM, but the approach was computationally infeasible for sampling the 1,075-dimensional TMVN distribution due to extremely low acceptance rates. The LOD-augmented GP produced an RMSE of 0.45, whereas the RMSE of our method was only 0.19. While the global approach cannot be computed as a gold-standard comparison method in this high-dimensional example, note that the nugget variance is 0.03, indicating a minimum prediction RMSE of 0.17. This highlights the benefits of properly taking the censored locations into consideration for posterior inference. In this example, the acceptance rate was approximately 2×10^{-5} and the sampling took less than 44 minutes. Combined with the results from Section 7.1, the VMET algorithm outlined in Algorithm 1 enables scalable (linear-complexity) computation for the partially censored MVN model in terms of parameter estimation and posterior inference, significantly outperforming the LOD-augmented GP and the SAEM approaches.

7.3 Analysis of groundwater contamination

We considered groundwater tetrachloroethylene concentrations from the United States Geological Survey (USGS) to demonstrate that our proposed VMET method can be used in combination with the censored MVN model to enhance the modeling of partially censored data. Tetrachloroethylene can be used in dry cleaning, manufacturing other chemicals, and cleaning metals, but exposure to tetrachloroethylene is harmful and may cause skin and respiratory problems. The data were collected at irregular locations across the United States over the time period 2000 to 2022. In this section, the locations $\{s_i \in \mathbb{R}^3\}$ are spatial-temporal coordinates consisting of longitudes, latitudes, and dates. Overall, there are $n = 24,701$ spatio-temporal responses, among which there are 20,730 censored responses due to detection limits. The detection thresholds are known and vary across spatio-temporal locations. Environmental contaminants are usually modeled using MVN distributions after a logarithm transformation (Helsel, 1990). During data preprocessing, we first applied a log-transform to both observations and detection thresholds. Next, we normalized the transformed observations and the detection thresholds with the mean and standard deviation of the transformed observations. The spatial and temporal coordinates were linearly scaled into the unit hypercube in \mathbb{R}^3 , with the two spatial coordinates scaled by the same constant.

The responses and detection thresholds after transformation were modeled by a partially censored MVN distribution with zero mean and a Matérn-1.5 kernel. We used one range parameter for longitude and latitude and another one for the temporal coordinate. Four parameters $(\sigma^2, \gamma_1, \gamma_2, \tau^2)$, namely variance, spatial range, temporal range, and nugget, were estimated by maximizing the likelihood (9) as described in Section 7.1. Notice that we used the chordal distance for our study since the spatial locations are all within the United States, where the chordal distance closely resembles the great-circle distance. For optimization, we set $m = 50$, MC sample size to 10^4 , and used the robust Nelder and Mead Algorithm (Nelder and Mead, 1965) native to R, which took approximately five hours to reach convergence; the parameters were estimated to be $(10.53, 0.09, 8.33, 0.09)$, indicating very strong temporal correlation.

We used the state of Texas as our region of interest for posterior inference. Specifically, our goal was to make predictions over a dense regular $0.13^\circ \times 0.11^\circ$ longitude-latitude grid covering Texas

on the last day of the dataset’s temporal range. Based on the predictions, we produced a ‘heatmap’ for the groundwater tetrachloroethylene concentrations in Texas. Conditional on all observed responses, we drew $N = 1,000$ samples of the TMVN distribution defined over the 691 censored spatio-temporal points that are located in Texas. Inference over the grid was made by kriging using all observed responses and the TMVN samples drawn by VMET. For comparison, we also considered predictions made by a GP using the augmented responses where censored responses were replaced by their LODs. The SAEM method was computationally infeasible for sampling from the 691-dimensional TMVN distribution, and it was hence excluded from our comparison. Figure 8 compares the heatmaps produced by the partially censored MVN model and the GP model. The

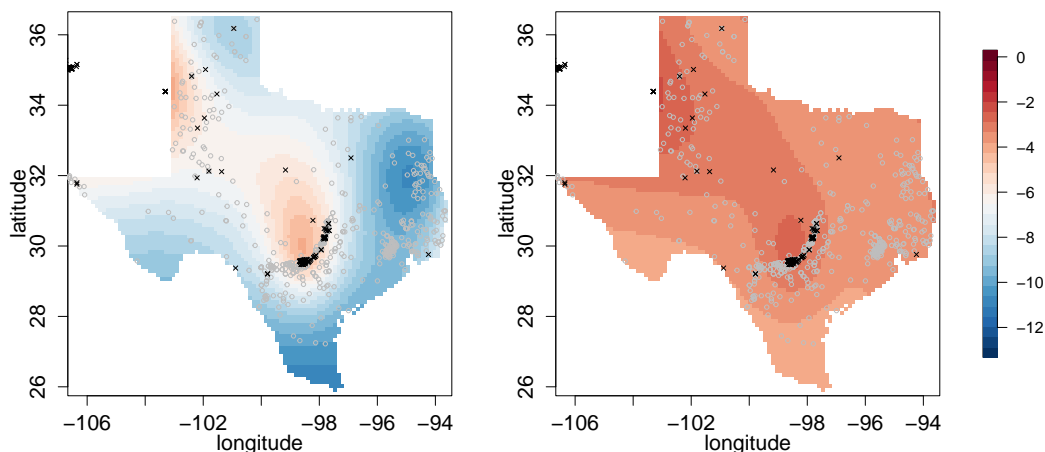


Figure 8: Inference (i.e., posterior means) on the logarithm of the groundwater tetrachloroethylene concentrations in Texas made by (left) partially censored MVN model and (right) LOD-augmented GP. Black crosses and grey circles denote the spatial locations of observed and censored data, respectively.

heatmap generated by the censored MVN model exhibits larger variations across space and more details than that produced by the LOD-augmented GP. Our prediction over the grid is likely to be more accurate based on the simulation results in Section 7.2. Furthermore, the inference produced by the GP with augmented data appeared unnatural, with predictions almost constant over large regions; hence, this approach may not be suitable for the logarithm of the contaminant levels (Helsel, 1990). The LOD-augmented GP is likely to have significantly overestimated the responses over the grid, which may have meaningful practical importance, as the two approaches differ in their assessment of where tetrachloroethylene concentrations are elevated and hence where mitigation may be necessary.

8 Conclusions

We proposed a linear-complexity method for estimating multivariate normal (MVN) probabilities and sampling truncated multivariate normal (TMVN) distributions at the same convergence and acceptance rate as the cubic-complexity state-of-the-art minimax exponential tilting (MET) method (Botev, 2017). Specifically, our proposed VMET approach improves over the existing MET in three aspects. First, we re-parameterized the MET integrand, reducing the complexity of each Monte Carlo (MC) sample from $\mathcal{O}(n^2)$ to $\mathcal{O}(n)$, where n is the dimension of the MVN probability.

Second, we proposed a linear-complexity estimator for the gradient and Hessian of the logarithm of the density ratio based on the Vecchia approximation, which reduced the computation cost of finding the proposal density used in the MET method by $\mathcal{O}(n^2)$. Finally, we introduced a Vecchia-based variable reordering that achieves the same effectiveness as the classic univariate reordering (Genz and Bretz, 2009) used in the MET method for improving the convergence/acceptance rate, while reducing its complexity by a factor of $\mathcal{O}(n)$. We also compared our proposed VMET to the tile-low-rank (TLR) method from Cao et al. (2021) that is currently the most scalable method for estimating MVN probabilities. In addition to higher estimation accuracy, VMET has lower time complexity (by a factor of $\mathcal{O}(n^{0.5})$) and was faster in our numerical examples with moderately large n . For sampling TMVN distributions, we proposed a ‘regional’ sampling scheme to make posterior inference more scalable. To demonstrate the practical usage of the VMET method, we considered a partially censored GP approach that can jointly model observed and censored data. Explicitly utilizing censored data substantially improves the model estimation and posterior inference of the underlying GP compared to GP regression with only the observed data or Markov-chain-Monte-Carlo-based methods. Our method has been shown to scale to tens of thousands of dimensions. Similar to other scalable methods (e.g., Cao et al., 2021; Genton et al., 2018; Nascimento and Shaby, 2022), our proposed VMET method amounts to an approximation to the covariance in the original MVN probability, and hence estimation bias is unavoidable. However, the Vecchia estimation bias is typically negligible relative to the MC errors for small values of the conditioning-set size m (e.g., 30 to 50), making the bias from the Vecchia approximation a worthwhile trade-off for much higher computation scalability. Furthermore, the Vecchia approximation used in VMET provides parallel-computation capability with respect to the number of responses n , in addition to the parallelization with respect to the sample size N .

One future research avenue is studying other families of proposal densities. Generally speaking, the design of proposal densities should consider how to 1) draw samples from the proposal density and 2) optimize the density function parameters. The convex-concave property, described in Proposition 3, for other families of proposal densities may no longer hold, necessitating innovative criteria for optimizing the proposal density, similar to (6).

An R implementation of our methods for variable reordering, computing MVN probabilities, and sampling TMVN distributions, along with code to reproduce our results, can be found at https://github.com/JCatwood/TMVN_Vecchia.

Acknowledgments

The authors were partially supported by National Science Foundation (NSF) Grants DMS–1654083 and DMS–1953005. Support for MK’s research was also provided by the Office of the Vice Chancellor for Research and Graduate Education at the University of Wisconsin–Madison with funding from the Wisconsin Alumni Research Foundation. We would like to thank Kyle Messier for providing the tetrachloroethylene data and for several helpful comments and discussions.

A Appendix/Proofs

Proof of Proposition 1. For notational simplicity, in this proof $c(i) = \{1, \dots, i-1\}$:

$$\begin{aligned}
E[x_i | \mathbf{x}_{1:i-1}] &= \boldsymbol{\Sigma}_{i,c(i)} \boldsymbol{\Sigma}_{c(i),c(i)}^{-1} \mathbf{x}_{c(i)} \\
&= \boldsymbol{\Sigma}_{i,c(i)} \boldsymbol{\Sigma}_{c(i),c(i)}^{-1} \mathbf{L}_{c(i),c(i)} \mathbf{y}_{c(i)} \\
&= \boldsymbol{\Sigma}_{i,c(i)} \mathbf{L}_{c(i),c(i)}^{-\top} \mathbf{L}_{c(i),c(i)}^{-1} \mathbf{L}_{c(i),c(i)} \mathbf{y}_{c(i)} \\
&= \mathbf{L}_{i,c(i)} \mathbf{y}_{c(i)},
\end{aligned}$$

where $\boldsymbol{\Sigma}_{i,c(i)}$ and $\mathbf{L}_{i,c(i)}$ are row vectors of length $i-1$, while $\mathbf{L}_{c(i),c(i)}$ and $\boldsymbol{\Sigma}_{c(i),c(i)}$ are matrices of dimension $(i-1) \times (i-1)$. Matrix inversions are taken with respect to the $(i-1)$ -dimensional matrices.

$$\begin{aligned}
\text{var}[x_i | \mathbf{x}_{1:i-1}] &= \boldsymbol{\Sigma}_{i,i} - \boldsymbol{\Sigma}_{i,c(i)} \boldsymbol{\Sigma}_{c(i),c(i)}^{-1} \boldsymbol{\Sigma}_{c(i),i} \\
&= \boldsymbol{\Sigma}_{i,i} - \boldsymbol{\Sigma}_{i,c(i)} \mathbf{L}_{c(i),c(i)}^{-\top} \mathbf{L}_{c(i),c(i)}^{-1} \boldsymbol{\Sigma}_{c(i),i} \\
&= \boldsymbol{\Sigma}_{i,i} - \|\mathbf{L}_{i,c(i)}\|^2 \\
&= \mathbf{L}_{i,i}^2
\end{aligned}$$

□

Proof of Proposition 2. Denote $\bar{c}(i) = [i, c(i)^\top]^\top$. Schäfer et al. (2021) showed that

$$\begin{aligned}
\mathbf{V}_{\bar{c}(i),i} &= (\boldsymbol{\Sigma}_{\bar{c}(i),\bar{c}(i)}^{-1})_{:,1} / \sqrt{(\boldsymbol{\Sigma}_{\bar{c}(i),\bar{c}(i)}^{-1})_{1,1}}, \\
\mathbf{V}_{-\bar{c}(i),i} &= \mathbf{0}.
\end{aligned}$$

On the other hand,

$$\begin{aligned}
(\boldsymbol{\Sigma}_{\bar{c}(i),\bar{c}(i)}^{-1})_{:,i} &= \begin{bmatrix} -\boldsymbol{\Sigma}_{c(i),c(i)}^{-1} \boldsymbol{\Sigma}_{c(i),i} (\boldsymbol{\Sigma}_{i,i} - \boldsymbol{\Sigma}_{i,c(i)} \boldsymbol{\Sigma}_{c(i),c(i)}^{-1} \boldsymbol{\Sigma}_{c(i),i})^{-1} \\ (\boldsymbol{\Sigma}_{i,i} - \boldsymbol{\Sigma}_{i,c(i)} \boldsymbol{\Sigma}_{c(i),c(i)}^{-1} \boldsymbol{\Sigma}_{c(i),i})^{-1} \end{bmatrix} \\
\mathbf{V}_{\bar{c}(i),i} &= \begin{bmatrix} \sqrt{(\boldsymbol{\Sigma}_{i,i} - \boldsymbol{\Sigma}_{i,c(i)} \boldsymbol{\Sigma}_{c(i),c(i)}^{-1} \boldsymbol{\Sigma}_{c(i),i})^{-1}} \\ -\boldsymbol{\Sigma}_{c(i),c(i)}^{-1} \boldsymbol{\Sigma}_{c(i),i} \sqrt{(\boldsymbol{\Sigma}_{i,i} - \boldsymbol{\Sigma}_{i,c(i)} \boldsymbol{\Sigma}_{c(i),c(i)}^{-1} \boldsymbol{\Sigma}_{c(i),i})^{-1}} \end{bmatrix} \\
E[x_i | \mathbf{x}_{1:i-1}] &= E[x_i | \mathbf{x}_{c(i)}] = \boldsymbol{\Sigma}_{i,c(i)} \boldsymbol{\Sigma}_{c(i),c(i)}^{-1} \mathbf{x}_{c(i)}.
\end{aligned}$$

Therefore,

$$E[x_i | \mathbf{x}_{1:i-1}] = -\mathbf{V}_{c(i),i}^\top / \mathbf{V}_{i,i} \mathbf{x}_{c(i)} = \mathbf{A}_{i,:} \mathbf{x}.$$

Based on Proposition 1, $L_{i,i}^2$ is the conditional variance $\text{var}[x_i | \mathbf{x}_{1:i-1}]$. $L_{i,i} = V_{i,i}^{-1}$ because \mathbf{L} is a lower-triangular matrix and $\mathbf{V} = \mathbf{L}^{-\top}$. Therefore, we have $\text{var}(x_i | \mathbf{x}_{1:i-1}) = \mathbf{V}_{i,i}^{-2}$. □

Proof of Proposition 3. Define $r_1(\gamma) := \log\{\Phi(b-\gamma) - \Phi(a-\gamma)\}$ and $r_2(\gamma) := \frac{1}{2}\gamma^2 + r_1(\gamma)$, where $a \in \mathbb{R}, b \in \mathbb{R}$ and $a < b$. First, we show that $r_1(\gamma)$ is concave while $r_2(\gamma)$ is convex. The same theoretical results used in Botev (2017) are also applicable here. Specifically, based on the properties of log-concave measures (Prékopa, 1973), $r_1(\gamma)$ is concave.

$$\begin{aligned}
r_2(\gamma) &= \log \int_a^b \exp(-\frac{1}{2}(x-\gamma)^2 + \frac{1}{2}\gamma^2) dx + c \\
&= \log \int_a^b \exp(-\frac{1}{2}x^2) \cdot \exp(x\gamma) dx + c,
\end{aligned}$$

which the moment generating function of a truncated univariate distribution up to a constant. Therefore, $r_2(\gamma)$ is convex.

Notice that when $a = \tilde{a}_i$, $b = \tilde{b}_i$, and $\gamma = \gamma_i$,

$$\frac{d^2 r_1}{d\gamma^2} = \Psi'_{i,i}, \quad \frac{d^2 r_2}{d\gamma^2} = 1 + \Psi'_{i,i}.$$

Therefore $-1 \leq \Psi'_{i,i} \leq 0$. Based on (8), which is derived in the proof of derivation in Proposition 4 below, we can see that $\frac{\partial^2 \psi}{\partial \mathbf{x}^2}$ is negative semidefinite and $\frac{\partial^2 \psi}{\partial \gamma^2}$ is positive semidefinite, which concludes the proof. \square

Proof of Proposition 4. The expression of ψ can be obtained by transforming $\sum_{i=1}^n \log \frac{\phi(y_i)}{\phi(y_i - \gamma_i)}$ with $y_i = (x_i - E[x_i | \mathbf{x}_{1:i-1}]) / \text{sd}(x_i | \mathbf{x}_{1:i-1})$:

$$\begin{aligned} \log \frac{\phi(y_i)}{\phi(y_i - \gamma_i)} &= -\gamma_i y_i + \frac{1}{2} \gamma_i^2 = -\gamma_i \frac{x_i - \mathbf{A}_{i,:} \mathbf{x}}{l_i} + \frac{1}{2} \gamma_i^2 \\ \psi &= \frac{1}{2} \|\boldsymbol{\gamma}\|^2 - (\mathbf{x} - \mathbf{A} \mathbf{x})^\top \mathbf{D}_1^{-1} \boldsymbol{\gamma} + \sum_i \log \left\{ \Phi(\tilde{b}_i - \gamma_i) - \Phi(\tilde{a}_i - \gamma_i) \right\}. \end{aligned}$$

Using the following relationship:

$$\begin{aligned} \frac{\partial \log \{ \Phi(\tilde{b}_i - \gamma_i) - \Phi(\tilde{a}_i - \gamma_i) \}}{\partial \gamma_i} &= \Psi_i, \\ \frac{\partial \Psi_i}{\partial \gamma_i} &= \Psi'_{i,i}, \\ \frac{\partial \log \{ \Phi(\tilde{b}_i - \gamma_i) - \Phi(\tilde{a}_i - \gamma_i) \}}{\partial \mathbf{x}} &= \mathbf{A}_{i,:}^\top l_i^{-1} \Psi_i, \\ \frac{\partial \Psi_i}{\partial \mathbf{x}} &= \mathbf{A}_{i,:}^\top l_i^{-1} \Psi'_{i,i}, \\ \frac{\partial \Psi_i}{\partial \gamma_j} &= 0 \quad \text{for } j \neq i, \end{aligned}$$

we can derive the gradient and Hessian of ψ :

$$\begin{aligned} \frac{\partial \psi}{\partial \mathbf{x}} &= -(\mathbf{I} - \mathbf{A})^\top \mathbf{D}_1^{-1} \boldsymbol{\gamma} + \mathbf{A}^\top \mathbf{D}_1^{-1} \boldsymbol{\Psi}, \quad \frac{\partial \psi}{\partial \boldsymbol{\gamma}} = \boldsymbol{\gamma} - \mathbf{D}_1^{-1} (\mathbf{x} - \boldsymbol{\mu}_c) + \boldsymbol{\Psi}, \\ \frac{\partial^2 \psi}{\partial \mathbf{x}^2} &= \mathbf{A}^\top \mathbf{D}_1^{-1} \boldsymbol{\Psi}' \mathbf{D}_1^{-1} \mathbf{A}, \quad \frac{\partial^2 \psi}{\partial \mathbf{x} \partial \boldsymbol{\gamma}} = -(\mathbf{I} - \mathbf{A})^\top \mathbf{D}_1^{-1} + \mathbf{A}^\top \mathbf{D}_1^{-1} \boldsymbol{\Psi}', \quad \frac{\partial^2 \psi}{\partial \boldsymbol{\gamma}^2} = \mathbf{I} + \boldsymbol{\Psi}'. \end{aligned}$$

\square

Proof of Proposition 5. This proof is a straightforward combination of Theorem 2 in Botev (2017), which makes no assumption on the covariance structure, and Proposition 1 in Katzfuss and Guinness (2021), which shows that any Vecchia approximation results in a valid joint MVN distribution. \square

References

- Bolin, D. and Lindgren, F. (2015). Excursion and contour uncertainty regions for latent gaussian models. *Journal of the Royal Statistical Society: Series B: Statistical Methodology*, pages 85–106.
- Botev, Z. (2017). The normal law under linear restrictions: simulation and estimation via minimax tilting. *Journal of the Royal Statistical Society. Series B (Statistical Methodology)*, pages 125–148.
- Cao, J., Genton, M. G., Keyes, D. E., and Turkiyyah, G. M. (2021). Exploiting low-rank covariance structures for computing high-dimensional normal and student-t probabilities. *Statistics and Computing*, 31:1–16.

- Cao, J., Genton, M. G., Keyes, D. E., and Turkiyyah, G. M. (2022a). tlmvnmvt: Computing high-dimensional multivariate normal and student-t probabilities with low-rank methods in r. *Journal of Statistical Software*, 101:1–25.
- Cao, J., Guinness, J., Genton, M. G., and Katzfuss, M. (2022b). Scalable Gaussian-process regression and variable selection using Vecchia approximations. *Journal of Machine Learning Research*, 23(348):1–30.
- Cao, J., Kang, M., Jimenez, F., Sang, H., Schäfer, F., and Katzfuss, M. (2023). Variational sparse inverse Cholesky approximation for latent Gaussian processes via double Kullback-Leibler minimization. *arXiv:2301.13303*.
- Croghan, C. and Egeghy, P. P. (2003). Methods of dealing with values below the limit of detection using sas. *Southern SAS User Group*, 22(24):22–24.
- Da Veiga, S. and Marrel, A. (2012). Gaussian process modeling with inequality constraints. In *Annales de la Faculté des sciences de Toulouse: Mathématiques*, volume 21, pages 529–555.
- Datta, A., Banerjee, S., Finley, A. O., and Gelfand, A. E. (2016). Hierarchical nearest-neighbor Gaussian process models for large geostatistical datasets. *Journal of the American Statistical Association*, 111(514):800–812.
- De Oliveira, V. (2005). Bayesian inference and prediction of gaussian random fields based on censored data. *Journal of Computational and Graphical Statistics*, 14(1):95–115.
- Durante, D. (2019). Conjugate bayes for probit regression via unified skew-normal distributions. *Biometrika*, 106(4):765–779.
- Genton, M. G., Keyes, D. E., and Turkiyyah, G. (2018). Hierarchical decompositions for the computation of high-dimensional multivariate normal probabilities. *Journal of Computational and Graphical Statistics*, 27(2):268–277.
- Genz, A. (1992). Numerical computation of multivariate normal probabilities. *Journal of Computational and Graphical Statistics*, 1(2):141–149.
- Genz, A. and Bretz, F. (2009). *Computation of Multivariate Normal and t Probabilities*, volume 195. Springer Science & Business Media.
- Helsel, D. R. (1990). Less than obvious-statistical treatment of data below the detection limit. *Environmental Science & Technology*, 24(12):1766–1774.
- Huser, R., Opitz, T., and Thibaud, E. (2017). Bridging asymptotic independence and dependence in spatial extremes using gaussian scale mixtures. *Spatial Statistics*, 21:166–186.
- Jimenez, F. and Katzfuss, M. (2023). Scalable Bayesian optimization using Vecchia approximations of Gaussian processes. In *International Conference on Artificial Intelligence and Statistics (AISTATS)*.
- Kang, M. and Katzfuss, M. (2023). Correlation-based sparse inverse Cholesky factorization for fast Gaussian-process inference. *Statistics and Computing*, 33(56):1–17.
- Katzfuss, M. and Guinness, J. (2021). A general framework for Vecchia approximations of Gaussian processes. *Statistical Science*, 36(1):124–141.
- Katzfuss, M., Guinness, J., Gong, W., and Zilber, D. (2020). Vecchia approximations of Gaussian-process predictions. *Journal of Agricultural, Biological, and Environmental Statistics*, 25(3):383–414.
- Katzfuss, M., Guinness, J., and Lawrence, E. (2022). Scaled Vecchia approximation for fast computer-model emulation. *SIAM/ASA Journal on Uncertainty Quantification*, 10(2):537–554.
- Liu, D. C. and Nocedal, J. (1989). On the limited memory bfgs method for large scale optimization. *Mathematical programming*, 45(1-3):503–528.

- Nascimento, M. and Shaby, B. A. (2022). A vecchia approximation for high-dimensional gaussian cumulative distribution functions arising from spatial data. *Journal of Statistical Computation and Simulation*, 92(9):1977–1994.
- Nelder, J. A. and Mead, R. (1965). A simplex method for function minimization. *The computer journal*, 7(4):308–313.
- Ordoñez, J. A., Bandyopadhyay, D., Lachos, V. H., and Cabral, C. R. (2018). Geostatistical estimation and prediction for censored responses. *Spatial statistics*, 23:109–123.
- Powell, M. J. (1970). A hybrid method for nonlinear equations. *Numerical methods for nonlinear algebraic equations*, pages 87–161.
- Prékopa, A. (1973). On logarithmic concave measures and functions. *Acta Scientiarum Mathematicarum*, 34:335–343.
- Saha, A., Datta, A., and Banerjee, S. (2022). Scalable predictions for spatial probit linear mixed models using nearest neighbor gaussian processes. *Journal of Data Science*, 20(4).
- Schäfer, F., Katzfuss, M., and Owhadi, H. (2021). Sparse Cholesky factorization by Kullback-Leibler minimization. *SIAM Journal on Scientific Computing*, 43(3):A2019–A2046.
- Schelin, L. and Sjöstedt-de Luna, S. (2014). Spatial prediction in the presence of left-censoring. *Computational Statistics & Data Analysis*, 74:125–141.
- Snelson, E. and Ghahramani, Z. (2007). Local and global sparse Gaussian process approximations. In *Artificial Intelligence and Statistics 11 (AISTATS)*.
- Stein, M. L. (2002). The screening effect in kriging. *Annals of Statistics*, 30(1):298–323.
- Stein, M. L. (2011). When does the screening effect hold? *Annals of Statistics*, 39(6):2795–2819.
- Stein, M. L., Chi, Z., and Welty, L. (2004). Approximating likelihoods for large spatial data sets. *Journal of the Royal Statistical Society: Series B*, 66(2):275–296.
- Vecchia, A. (1988). Estimation and model identification for continuous spatial processes. *Journal of the Royal Statistical Society, Series B*, 50(2):297–312.
- Zhang, H. and El-Shaarawi, A. (2010). On spatial skew-gaussian processes and applications. *Environmetrics: The official journal of the International Environmetrics Society*, 21(1):33–47.